LINEAR ELASTIC FRACTURE MECHANICS AS A LIMIT - CASE OF STRAIN - SOFTENING INSTABILITY

Alberto Carpinteri

Estratto da:

MECCANICA

Journal of the Italian Association of Theoretical and Applied Mechanics AIMETA

Vol. 23 • No. 3 • September 1988

PITAGORA EDITRICE BOLOGNA

MECCANICA
23 (1988), 160-165

LINEAR ELASTIC FRACTURE MECHANICS AS A LIMIT - CASE OF STRAIN - SOFTENING INSTABILITY*

Alberto Carpinteri**

SOMMARIO. Si dimostra come la scala dimensionale, la snellezza e il grado di iperstaticità, influenzino in modo fondamentale il comportamento globale di una struttura. Tale comportamento potrà variare da duttile a fragile, allorché si prendano in considerazione l'incrudimento negativo e la localizzazione della deformazione. Il comportamento fragile consiste in una instabilità interna lungo la curva carico-spostamento, acquistando il ramo discendente una pendenza positiva (snap-back). Tale ramo virtuale può venire rilevato sperimentalmente solo nel caso in cui il processo di carico venga pilotato da una funzione monotona crescente del tempo (es., la larghezza della fessura). Altrimenti, la capacità di carico presenterà una discontinuità con un salto negativo. Qualora il comportamento oltre il carico massimo venga tenuto sotto controllo sino alla separazione completa del provino, l'area compresa tra la curva carico-spostamento e l'asse dello spostamento, rappresenta l'energia dissipata nel processo di fessurazione. Viene infine fornita una giustificazione sia alla diminuzione della resistenza a trazione che all'aumento della tenacità alla frattura, che si verificano all'aumentare della dimensione del provino, sulla base dei concetti dell'Analisi Dimensionale. A causa delle diverse dimensioni fisiche di resistenza $[FL^{-2}]$ e tenacità $[FL^{-1}]$, i valori reali di tali due proprietà intrinseche del materiale possono essere determinati esattamente soltanto con provini di dimensione relativamente grande.

SUMMARY. Size-scale, slenderness and degree of redundancy are shown to have a fundamental impact on the global structural behaviour, which can range from ductile to brittle when strain softening and localization are taken into account. The brittle behaviour involves an internal instability in the load-deflection path, which shows a positive slope in the softening branch. This virtual branch is revealed only if the loading process is controlled by a monotonically increasing time function (e.g., the crack opening displacement). Otherwise, the loading capacity shows discontinuity with a negative jump. When the post-peak behaviour is kept under control up to the complete structure separation, the area bounded by the load-deflection curve and the deflection axis represents the energy dissipated in the fracture process. A general explanation of the well-known decrease in apparent strength and increase in fracture toughness by increasing the specimen size is given in terms of dimensional analysis. Due to the different physical dimensions of strength $[FL^{-2}]$ and toughness $[FL^{-1}]$, the actual values of these two intrinsic material properties may be found exactly only with comparatively large specimens.

1. INTRODUCTION

The curvature *localization* for bent beams is related to the fracture toughness of the material. Even if no initial cracks are assumed to exist in the structure, the fracture mechanics concepts are applicable. Size-scale, slenderness and degree of redundancy are shown to exert a fundamental influence on the global structure behaviour, which can range from ductile to brittle when *softening* is taken into account.

When a bifurcation (or internal instability) of the load-deflection equilibrium path occurs, the softening slope becomes positive. If the loading process is deflection-controlled, the loading capacity of the beam shows discontinuity with a negative jump. This dreadful event is favoured by large size-scale, high slenderness and/or low degree of redundancy [1].

Strain localization and softening are then considered in order to analyze the three-point bending of rectangular slabs. Even in this case, for large sizes and high slendernesses, the slope of the global softening branch appears to be positive. This branch is not virtual only if the loading process is controlled by a monotonically increasing time function. When the post-peak behaviour is kept under control up to the complete structure separation, the area outlined by the load-deflection curve and the deflection axis represents the product of fracture toughness ($\mathcal{G}_{IC}$) by the initial cross-section area.

An explanation of the well-known decrease in apparent strength by increasing specimen size is given, without making the usual statistical Weibull assumptions and assuming the existence of initial cracks and defects. It has been proved that the actual strength of the material can be obtained only with specimens of infinite size, where the influence of heterogeneity becomes unimportant. With the real specimens, an apparent strength higher than the actual one is consistently found.

A cohesive crack model is eventually applied in order to analyze the three-point bending of initially cracked rectangular slabs. Once more, an internally unstable post-peak behaviour occurs for large sizes. This may be kept

* Paper presented at the 8th National Conference of the Italian Association of Theoretical and Applied Mechanics, Torino, September 29 - October 3, 1986.

** Professor of Structural Mechanics, Politecnico di Torino, Torino, Italy.

under control by the crack mouth opening displacement, which is an increasing function of time, even when load and deflection decrease following the softening branch with positive slope. The area marked out by the load-deflection curve and the deflection axis is the product of fracture toughness ($\mathcal{G}_{IC}$) by initial ligament area.

An explanation of the recurrent experimental increase in fracture toughness by increasing specimen size is provided, without resorting to the usual non-linear theories and the energy dissipation in the crack tip plastic zones. It has been proved that the actual fracture toughness (K_{IC}) of the material can be obtained only with specimens of infinite size. With the real specimens, a fictitious fracture toughness lower than the actual one is consistently measured [2].

2. STRAIN-SOFTENING INSTABILITY OF BENT BEAMS

Let us consider a linear elastic moment-curvature relation (Fig. 1-a) associated with a linear softening moment-rotation law (Fig. 1-b). The area below the moment-rotation curve represents the energy dissipated by the softening hinge until this becomes a free-rotation hinge without resisting moment. This area is equal to the product of the separation energy or strain energy release rate, $\mathcal{G}_{IC}$, by the cross-section area, A:

$$\frac{1}{2} M_u \varphi_0 = \mathcal{G}_{IC} A. \tag{1}$$

For the statically determined beam in Fig. 2-a the central deflection is:

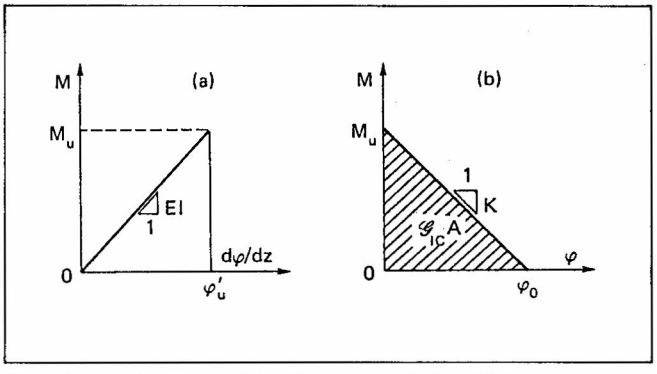

Fig. 1. Moment-curvature (a) and moment-rotation (b) law.

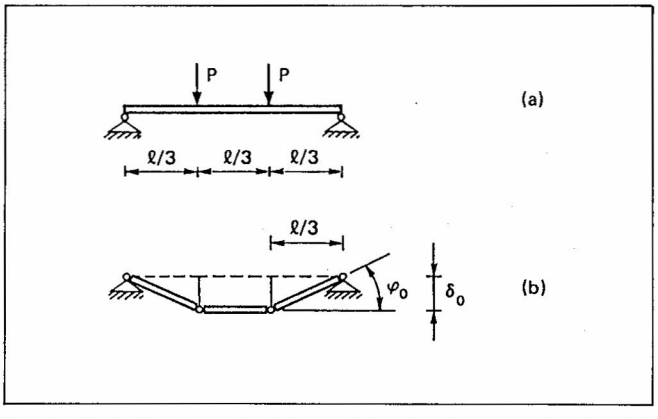

Fig. 2. Statically determined beam (a) and collapse mechanism (b).

$$\delta = \frac{23}{648} \frac{P\ell^3}{EI}, \tag{2}$$

E being the Young's modulus of the material and I the inertial moment of the cross-section of the beam. If the cross-section is assumed to be rectangular with depth b and thickness t, the ultimate strength load P_u is given by:

$$M_u = \sigma_u \frac{tb^2}{6} = P_u \frac{\ell}{3}, \tag{3}$$

where σ_u is the ultimate tensile strength of the material. From eqs. (2) and (3) it is possible to obtain the deflection in the ultimate strength condition:

$$\delta_u = \frac{23}{108} \frac{\epsilon_u \ell^2}{b}, \tag{4}$$

where $\epsilon_u = \sigma_u / E$.

If, in the ultimate strength condition, two softening hinges form at the load application points, the bending moments in the hinges and, generally, in the beam decrease. At this intermediate stage, the hinge rotations increase, whereas the beam curvatures decrease. Central deflection increases or decreases with the prevalence of hinge rotations or beam curvatures respectively. Eventually, when hinge rotations achieve the limit value φ_0, the beam is completely unloaded with $P = 0$ and $\delta = \delta_0 = \varphi_0 \ell/3$ (Fig. 2-b).

Rearranging of eq. (2) gives:

$$P = \frac{648}{23} \frac{EI}{\ell^3} \delta, \quad \text{for } \delta \leqslant \delta_u, \tag{5}$$

while the condition of complete load relaxation reads:

$$P = 0, \text{ for } \delta \geqslant \delta_0. \tag{6}$$

When $\delta_0 > \delta_u$, the softening process is stable only if deflection-controlled, since the slope $dP/d\delta$ is negative (Fig. 3-a). When $\delta_0 = \delta_u$, the slope $dP/d\delta$ is not defined and a drop in the loading capacity occurs, even if the loading is deflection-controlled (Fig. 3-b). Eventually, when $\delta_0 < \delta_u$, the slope $dP/d\delta$ becomes positive (Fig. 3-c) and the same negative jump occurs as that shown in Fig. 3-b. Therefore internal instability occurs for [3]:

$$\frac{\varphi_0 \ell}{3} \leqslant \frac{23}{108} \frac{\epsilon_u \ell^2}{b}, \tag{7}$$

i.e., for:

$$\frac{\varphi_0}{\epsilon_u \lambda} \leqslant \frac{23}{36}, \tag{8}$$

where $\lambda = \ell/b$ is the beam slenderness. Recalling eqs. (1) and (3), the following is obtained:

$$\varphi_0 = 12 \frac{\mathcal{G}_{IC}}{\sigma_u b} = 12\, s_E, \tag{9}$$

where:

$$s_E = \frac{\mathcal{G}_{IC}}{\sigma_u b} \tag{10}$$

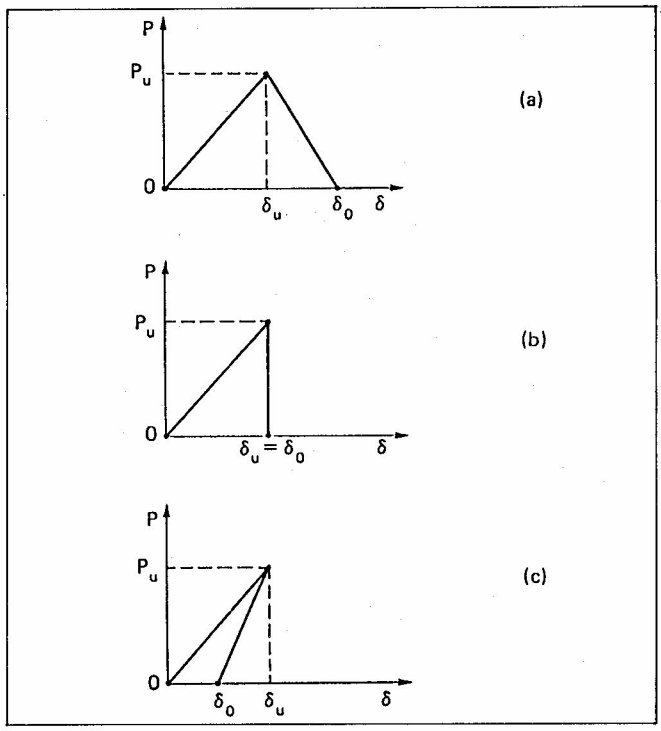

Fig. 3. Load-deflection diagram: (a) externally unstable; (b) and (c) internally unstable.

is the brittleness number defined in [4], which is a function of the material properties and structural size-scale.

Eqs. (8) and (9) provide the *brittleness condition:*

$$B = \frac{s_E}{\epsilon_u \lambda} \leqslant \frac{23}{432} \cong \frac{1}{18.78} . \tag{11}$$

For the statically undetermined beam in Fig. 4, the condition of internal instability was solved by Maier in [1]. It reads:

$$\alpha = \frac{K\ell}{2EI} \geqslant 1.8, \tag{12}$$

with $K = M_u/\varphi_0$ (Fig. 1-b). Recalling eqs. (1) and (3), eq. (12) becomes:

$$\frac{\epsilon_u \lambda}{12\, s_E} \geqslant 1.8, \tag{13}$$

and a *brittleness condition* is obtained also in this case:

$$B = \frac{s_E}{\epsilon_u \lambda} \leqslant \frac{1}{12 \times 1.8} = \frac{1}{21.60} . \tag{14}$$

Comparing eqs. (11) and (14), it can be concluded that the statically determined beam in Fig. 2 is comparatively brittler than the statically undetermined beam in Fig. 4. Size-scale, slenderness and degree of redundancy are shown to have a fundamental influence on the global structure behaviour. Brittleness is favoured by large size, high slenderness and/or low degree of redundancy.

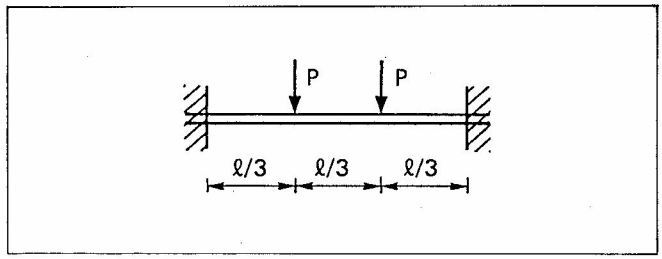

Fig. 4. Statically undetermined beam.

3. STRAIN LOCALIZATION AND APPARENT STRENGTH OF INITIALLY UNCRACKED SLABS

Strain localization is considered in a three-point bending slab of elastic-softening material (Fig. 5, $a_0 = 0$). A displacement discontinuity forms locally when the principal stress achieves the ultimate tensile strength σ_u. At the same time, cohesive forces rise between the two opposite crack surfaces. These forces depend on the distance of the interacting surfaces: by increasing the distance w, the cohesive forces decrease until they vanish for $w \geqslant w_c$. In line with the linear elastic $\sigma - \epsilon$ law (Fig. 6-a), a linear $\sigma - w$ cohesive law is assumed (Fig. 6-b). The energy necessary to produce a unit crack surface is then:

$$\mathcal{G}_{IC} = \int_0^{w_c} \sigma \, dw = \frac{1}{2} \sigma_u w_c .$$

The real crack tip is defined as the point where displacement discontinuity is equal to the interaction threshold w_c, whereas the fictitious crack tip is defined as the point where normal stress attains its maximum value σ_u and the displacement discontinuity vanishes (Fig. 7).

The displacement discontinuities on the midline may be expressed as follows:

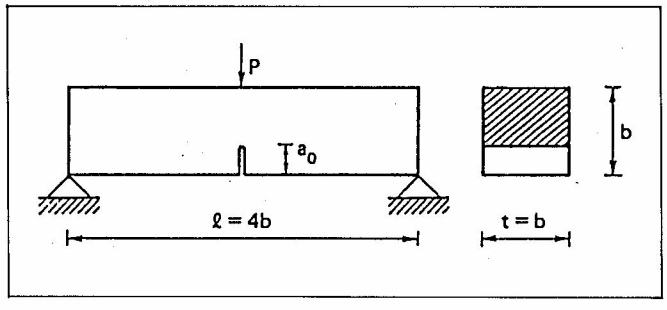

Fig. 5. Three-point bending slab with initial crack.

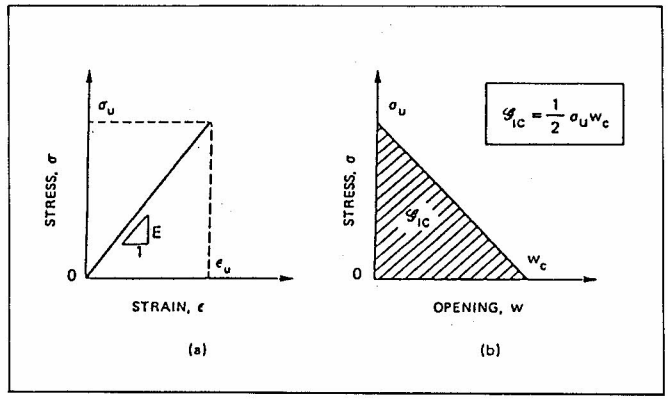

Fig. 6. Stress-strain (a) and stress-crack opening displacement (b) constitutive laws.

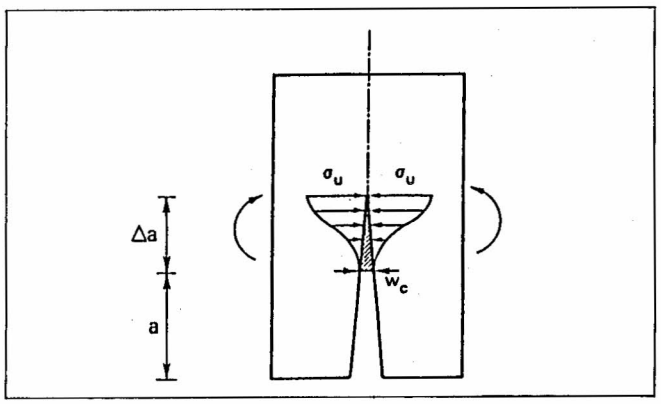

Fig. 7. Stress distribution across the cohesive zone: real and fictitious crack tips.

$$w(x) = \int_0^b K(x, y)\, \sigma(y)\, dy + C(x)P + \Gamma(x), \tag{16}$$

for $0 \leqslant x < b$,

where K and C are the influence functions of cohesive forces and external load respectively, and Γ are the crack openings due to the specimen weight. If a stress-free crack of length a has developed with a cohesive zone of length Δa, the following additional conditions are to be taken into account:

$$\sigma(y) = 0, \quad \text{for} \quad 0 \leqslant y \leqslant a, \tag{17-a}$$

$$\sigma(y) = \sigma_u \left[1 - \frac{w(y)}{w_c}\right], \quad \text{for } a \leqslant y \leqslant (a + \Delta a), \tag{17-b}$$

$$w(x) = 0, \quad \text{for} \quad (a + \Delta a) \leqslant x < b. \tag{17-c}$$

Eqs. (16) and (17) can be rearranged as follows:

$$w(x) = \int_a^{a+\Delta a} K(x, y) \left[1 - \frac{w(y)}{w_c}\right] \sigma_u\, dy +$$

$$+ \int_{a+\Delta a}^b K(x, y)\, \sigma(y)\, dy + C(x)\, P + \Gamma(x),$$

for $0 \leqslant x \leqslant (a + \Delta a)$, (18-a)

$$w(x) = 0, \quad \text{for} \quad (a + \Delta a) \leqslant x < b. \tag{18-b}$$

Eqs. (18-a) and (18-b) are two integral equations for the unknown functions σ and w. These equations can be discretized by considering n points on the midline between the bottom and the top of the beam [5].

The additional unknown parameter P can be determined, since both equations are valid for $x = a + \Delta a$, i.e. at the fictitious crack tip.

On the other hand, the beam deflection is given by:

$$\delta = \int_0^b C(y)\, \sigma(y)\, dy + D_p P + D_\gamma, \tag{19}$$

where D_p is the deflection for $P = 1$ and D_γ is the deflection due to the specimen weigth.

A numerical procedure is implemented to simulate a loading process whereby the fictitious crack depth is increased step by step [5]. Real (or stress-free) crack depth,external load and deflection are obtained at each step as a result of an iterative computation. Some dimensionless load-deflection diagrams for a concrete-like material are plotted in Fig. 8-a, with $a_0/b = 0.0$, $\epsilon_u = 0.87 \times 10^{-4}$, $\nu = 0.1$, $t = b$, $\ell = 4b$, and by varying the non-dimensional number [4]:

$$s_E = \frac{\mathcal{G}_{IC}}{\sigma_u b} = \frac{w_c}{2b}. \tag{20}$$

The specimen behaviour is brittle (or internally unstable) for low s_E numbers, i.e., for low fracture toughnesses $\mathcal{G}_{IC}$, high tensile strengths, σ_u, and/or large sizes b. For $s_E \lesssim \lesssim 10.45 \times 10^{-5}$, the P-δ curve exhibits a positive slope in the softening branch and a catastrophic event occurs if the loading process is deflection-controlled. This indenting branch is not virtual only if the loading process is controlled by a monotonically increasing time function, such as the displacement discontinuity across the crack. When the post-peak behaviour is kept under control up to the complete structure separation, the area bounded by the load-deflection

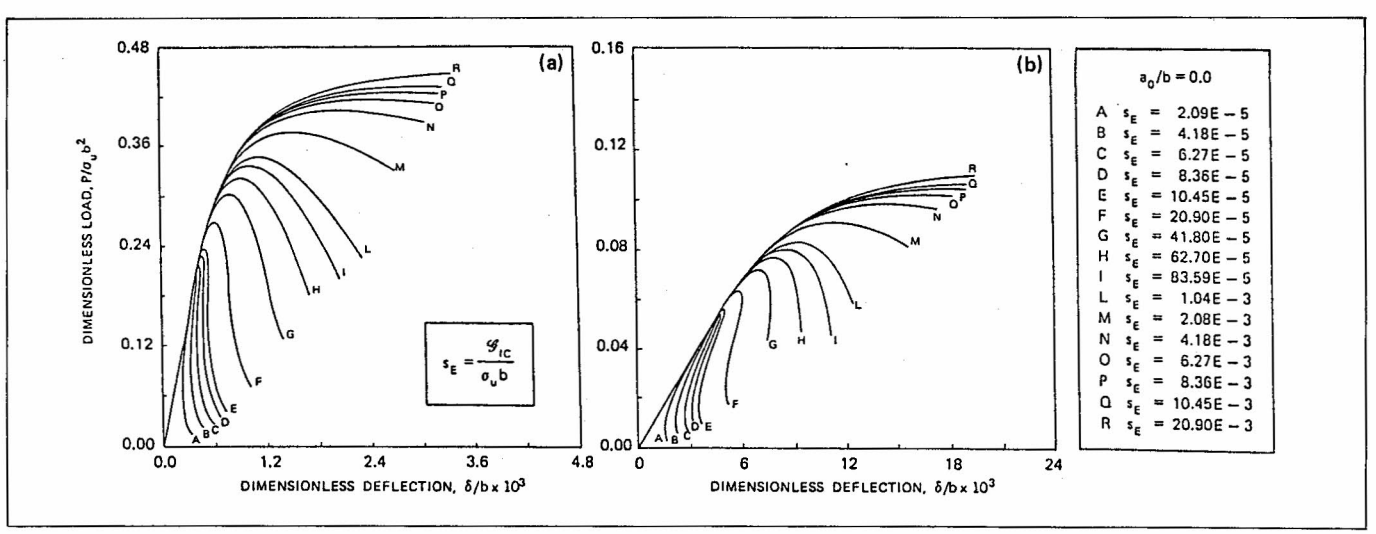

Fig. 8. Load-deflection diagrams of initially uncraked slabs: (a) $\ell = 4b$; (b) $\ell = 16b$.

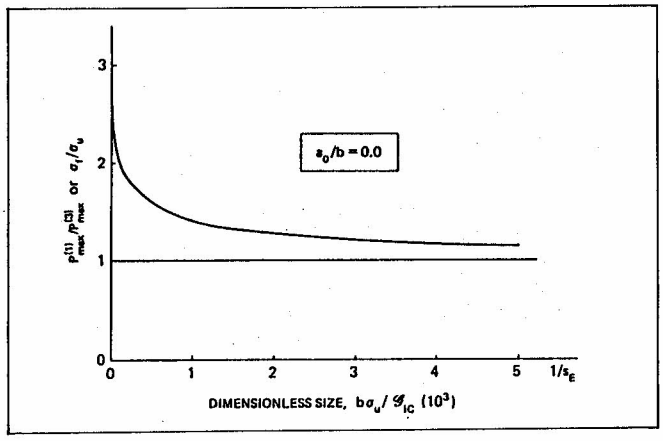

Fig. 9. Decrease in apparent strength with increasing specimen size.

curve and the deflection-axis is the product of fracture toughness, $\mathcal{G}_{IC}$, by initial cross-section area, bt.

The diagrams in Fig. 8-b refer to an higher beam slenderness, $\ell = 16\,b$. The same brittleness increase with decreasing s_E is obtained as previously, but in this case it is easier to achieve the internal instability of the system, when $s_E \lesssim \lesssim 62.70 \times 10^{-5}$.

The maximum loading capacity $P^{(1)}_{max}$ of initially uncracked specimens with $\ell = 4b$ is obtained from Fig. 8-a. On the other hand, the maximum load $P^{(3)}_{max}$ of ultimate strength is given by:

$$P^{(3)}_{max} = \frac{2}{3}\,\frac{\sigma_u t b^2}{\ell}. \tag{21}$$

The values of the ratio $P^{(1)}_{max}/P^{(3)}_{max}$ may also be regarded as the ratio of the apparent tensile strength, σ_f (given by the maximum load $P^{(1)}_{max}$ and applying eq. (21)) to the actual tensile strength σ_u (considered to be a material constant). It is evident from Fig. 9 that the results of the cohesive crack model tend to be similar to those of the ultimate strength analysis for low s_E values:

$$\lim_{s_E \to 0} P^{(1)}_{max} = P^{(3)}_{max}. \tag{22}$$

Therefore, only for comparatively large specimen sizes can the tensile strength σ_u be obtained as $\sigma_u = \sigma_f$. With the usual laboratory specimens, an apparent strength higher than the actual one is always found.

4. COHESIVE CRACK PROPAGATION AND FICTITIOUS FRACTURE TOUGHNESS OF INITIALLY CRACKED SLABS

The mechanical behaviour of three-point bending slabs with initial craks (Fig. 5) is investigated on the basis of the same cohesive numerical model described in the previous section. Some dimensionless load-deflection diagrams are given in Fig. 10, for $a_0/b = 0.5, \varepsilon_u = 0.87 \times 10^{-4}$, $\nu = 0.1$, $t = b$, $\ell = 4b$, and for various values of the brittleness number s_E (see eq. (20)). The initial crack makes the specimen bahaviour more ductile than in the case of initially uncracked specimen. For the set of s_E numbers considered in Fig. 10, no internal instability occurs.

The area delimited by the load-deflection curve and the deflection-axis is the product of fracture toughness, $\mathcal{G}_{IC}$, by initial ligament area, $(b - a_0)t$. The areas below the P-δ curves are thus proportional to the respective s_E numbers, as is shown in Fig. 10 as well as in Fig. 8. This simple result is based on the assumption that energy dissipation occurs only on the fracture surface, whereas in reality energy is also dissipated in a damage volume around the crack tip, as was assumed by Carpinteri and Sih in [6]. On the other hand, the cohesive crack assumption is more than acceptable for slender beams, where bending prevails over shear and energy dissipation is concentrated in a very narrow crack band [7].

The maximum loading capacity $P^{(1)}_{max}$ according to the cohesive crack model, is obtained from Fig. 10. On the other hand, the maximum load $P^{(2)}_{max}$ of brittle fracture can be obtained from the Linear Elastic Fracture Mechanics

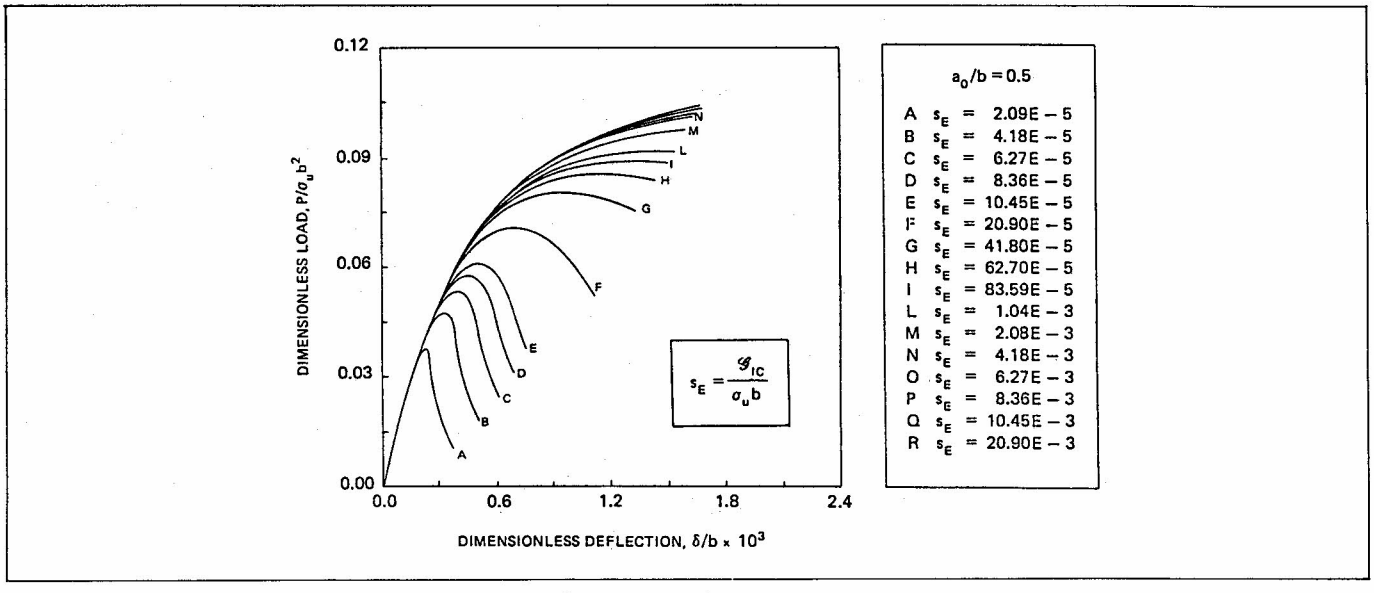

Fig. 10. Load-deflection diagrams of initially cracked slabs ($\ell = 4b$, $a_0 = b/2$).

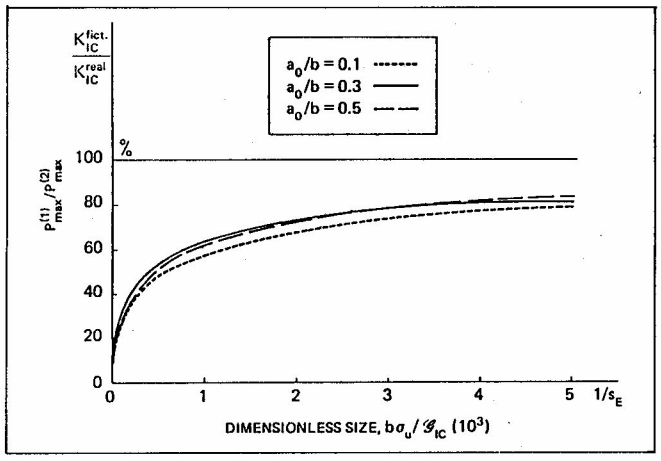

Fig. 11. Increase in fictitious fracture toughness by increasing the specimen size.

equation [8]:

$$K_{IC} = \frac{P_{max}^{(2)}\,\ell}{tb^{3/2}}\, f\left(\frac{a_0}{b}\right),$$

$$f\left(\frac{a_0}{b}\right) = 2.9\left(\frac{a_0}{b}\right)^{1/2} - 4.6\left(\frac{a_0}{b}\right)^{3/2} + 21.8\left(\frac{a_0}{b}\right)^{5/2} -$$

$$- 37.6\left(\frac{a_0}{b}\right)^{7/2} + 38.7\left(\frac{a_0}{b}\right)^{9/2}, \qquad (23)$$

with $K_{IC} = \sqrt{\mathcal{G}_{IC} E}$ (plane stress condition).

The values of the ratio $P_{max}^{(1)}/P_{max}^{(2)}$ are provided in Fig. 11 as functions of the inverse of the brittleness number s_E. This ratio can also be regarded as the ratio of the fictitious fracture toughness (given by the maximum load $P_{max}^{(1)}$) to the actual fracture toughness (considered to be a material constant).

It is evident that, for low s_E numbers, the results of the cohesive crack model are similar to those of Linear Elastic Fracture Mechanics:

$$\lim_{s_E \to 0} P_{max}^{(1)} = P_{max}^{(2)}, \qquad (24)$$

and, therefore, maximum loading capacity can be predicted by applying the simple condition $K_I = K_{IC}$. It appears that the actual fracture toughness K_{IC} of the material can be obtained only with very large specimens. In fact, with laboratory specimens, a fictitious fracture toughness lower than the actual one is always measured.

5. CONCLUSIONS

Recalling Figs. 9 and 11 once again, it can be stated that the smaller the brittleness number s_E, the more accurately the bifurcation reproduces the perfectly brittle ultimate strength instability ($a_0 = 0$) or the Linear Elastic Fracture Mechanics instability ($a_0 \neq 0$).

Therefore, ultimate tensile strength σ_u or fracture toughness K_{IC} can be obtained exactly only with very large (initially uncracked or cracked respectively) specimens. On the other hand, the critical value $\mathcal{G}_{IC}$ of strain energy release rate may be derived from the area delimited by the load-deflection curve and the deflection-axis for any specimen size.

ACKNOWLEDGEMENTS

The numerical results reported in the present paper were obtained in a joint research program between ENEL-CRIS-Milano and the University of Bologna.

Received: November 14, 1987; in revised form: March 14, 1988.

REFERENCES

[1] MAIER G., *Sul comportamento flessionale instabile nelle travi inflesse elastoplastiche,* Istituto Lombardo, Accademia di Scienze e Lettere, Rendiconti, Classe di Scienze (A), Vol. 102, pp. 648-677, 1968.

[2] CARPINTERI A., *Notch sensitivity in fracture testing of aggregative materials,* Engineering Fracture Mechanics, 16, pp. 467-481, 1982.

[3] CARPINTERI A., *Limit analysis for elastic-softening structures: scale and slenderness influence on the global brittleness,* Structure and Crack Propagation in Brittle Matrix Composite Materials, Euromech Colloquium No. 204, November 12-15, 1985, Jablonna (Warsaw), edited by A.M. Brandt, Elsevier Applied Science Publishers, pp. 497-508, 1986.

[4] CARPINTERI A., *Interpretation of the Griffith instability as a bifurcation of the global equilibrium,* Application of Fracture Mechanics to Cementitious Composites, NATO Advanced Research Workshop, September 4-7, 1984, Northwestern University, edited by S.P. Shah, Martinus Nijhoff Publishers, pp. 287-316, 1985.

[5] CARPINTERI A., DI TOMMASO A., FANELLI M., *Influence of material parameters and geometry on cohesive crack propagation,* International Conference on Fracture Mechanics of Concrete, Lausanne, October 1-3, 1985, edited by F.H. Wittmann, Elsevier Science Publishers B.V., pp. 117-135, 1986.

[6] CARPINTERI A., SIH G.C., *Damage accumulation and crack growth in bilinear materials with softening,* Theoretical and Applied Fracture Mechanics, 1, pp. 145-159, 1984.

[7] BAZANT Z.P., CEDOLIN L., *Blunt crack band propagation in finite element analysis,* Journal of the Engineering Mechanics Division, ASCE, 105, pp. 297-315, 1979.

[8] Standard Method of Test for Plane Strain Fracture Toughness of Metallic Materials, E 399-74, ASTM.